

Attitude estimation from polarimetric cameras

Mojdeh Rastgoo¹, Désire Sidibé¹, Ralph Seulin¹, Cedric Demonceaux¹, Olivier Morel¹

Abstract— In the robotic field, navigation and path planning applications benefit from a wide range of visual systems (e.g. perspective cameras, depth cameras, catadioptric cameras, etc.). In outdoor conditions, these systems capture information in which sky regions cover a major segment of the images acquired. However, sky regions are discarded and are not considered as visual cue in vision applications. In this paper, we propose to estimate attitude of Unmanned Aerial Vehicle (UAV) from sky information using a polarimetric camera. Theoretically, we provide a framework estimating the attitude from the skylight polarized patterns. We showcase this formulation on simulated data sets which proved the benefit of using polarimetric sensors along with other visual sensors in robotic applications.

I. INTRODUCTION

Large-field cameras and lenses (e.g. omnidirectional and fisheye cameras) are popular in robotic applications due to their ability to provide large field of view (up to 360°), extending the amount of visual information. It is the main reason for which they have been adopted for a broad range of tasks such as visual odometry [?], navigation [?], simultaneous localization and mapping (SLAM) [?], and tracking [?]. With those systems, sky regions in the images acquired represent a large segment of information which are usually discarded. Here, we show that polarimetric information can be extracted from those regions and used in robotic applications.

Sun position, stars and sky patterns are hold as navigational cues for the past centuries. Indeed, before the discovery of magnetic compass, these natural cues have been the solitary source of navigation used by our ancestors [?, ?]. Similarly, some insects used the skylight polarized pattern created by the scattered sunlight to navigate in their environment [?, ?]. For instance, desert ants (*cataglyphis*), butterflies and dragonflies among others, are able to navigate through their paths, efficiently and robustly by using the polarized pattern of sky, despite their small brains [?, ?, ?].

Acknowledging the nature, numerous studies have been conducted on polarized skylight pattern [?, ?, ?, ?, ?, ?, ?, ?, ?, ?, ?, ?]. These studies are generally reported in the optic field. They focus on estimating the solar azimuth angle by creating a sort of compass. Estimating polarized patterns have been, however, a difficult and complex task. The primary studies report the use of several photodiodes [?, ?, ?, ?, ?], or of multiple cameras [?, ?, ?] or manually rotating filters [?, ?, ?, ?]. As a consequence of those troublesome setups, robotic applications are not benefiting from

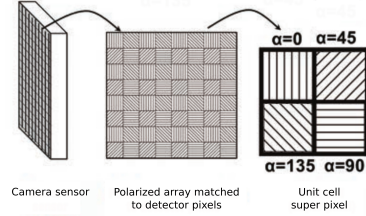


Fig. 1. Structure of DoFP sensors. Using this sensor four linearly polarized image corresponding to the four orientation of the polarized filters is acquired instantly

the advantages of polarized patterns, as attested by the lack of polarized sensors used in Unmanned Aerial Vehicle (UAV). However, the recent introduction of division-of-focal-plane (DoFP) micropolarizer cameras has offered an alternative solution [?, ?, ?]. In such cameras a micropolarizer filter array, composed of a pixelated polarized filters oriented at different angles, is aligned with a detector array. Thus, linear polarization information are simultaneously acquired taking a single image. Here, we use a DoFP coupled with a fisheye lens to exploit the polarized information of sky region to estimate vehicle attitude.

In this paper, Sect. II presents the specificity of the camera used and the adaptation required for our robotic application. The remainder of the paper is organized as follows: Sect. III introduces the concepts of polarization by scattering, Rayleigh model and the relation with attitude estimation while our formulation to estimate attitude is presented in Sect. IV. Experiments and implementation details are given in Sect. V, and finally discussions and conclusions are drawn in Sect. VI.

II. SETTING THE POLARIMETRIC CAMERA FOR ROBOTICS

As mentioned previously, in this work we use a DoFP polarimetric camera, to be exact *IMPREX Bobcat GEV polarimetric camera*. This camera has the advantage to capture four different linearly polarized measure in one image, due to their micropolarizer and pixelated polarized filter array (see Fig. 1). Therefore each capture image leads to four linearly polarized sub-image I_0 , I_{45} , I_{135} , I_{90} . Using these four measurements, the polarized state of the incident light is calculated in terms of stokes parameters [?], which are used thereafter to calculate polarized parameters such as angle of polarization (AoP) and degree of linear polarization (DoPl) (see Eq. 1).

*This work was not supported by any organization

¹ Université de Bourgogne Franche-Comté, 71200 Le Creusot, France
olivier.morel@u-bourgogne.fr

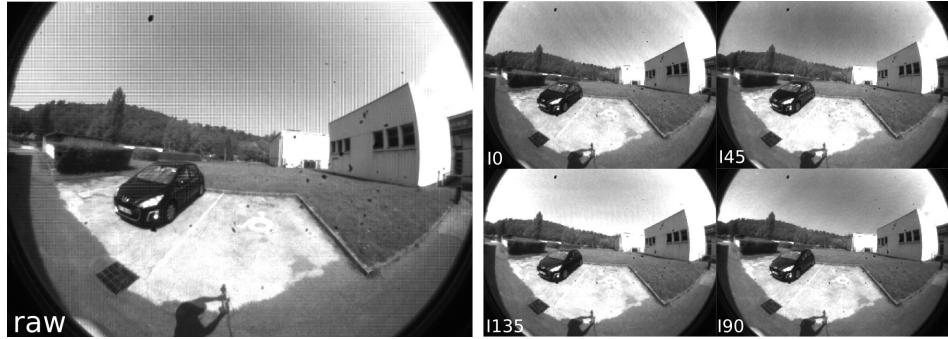


Fig. 2. A raw image captured with fisheye lens, and the extracted four linearly polarized images ($I_0, I_{45}, I_{135}, I_{90}$)

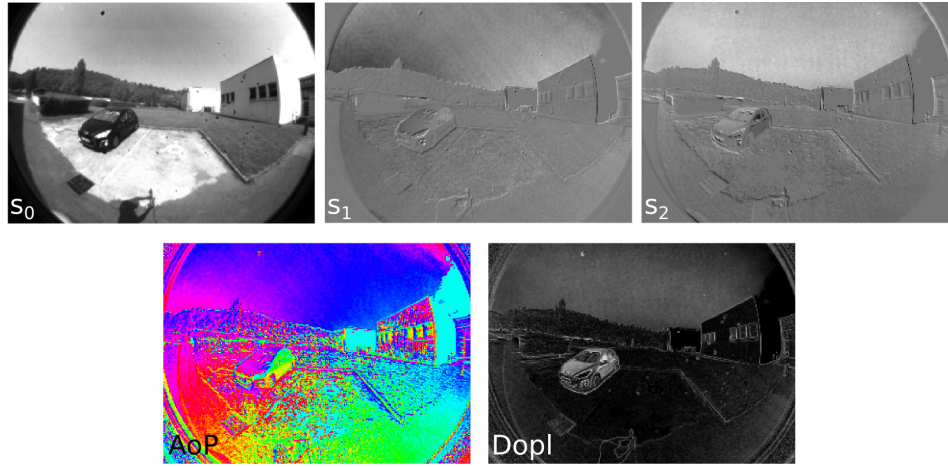


Fig. 3. Calculated stokes parameters (s_0, s_1, s_2), AoP, and DoPl images. For visualization purpose, AoP is represented in *hsv* color space.

$$\begin{aligned} s_0 &= (I_0 + I_{45} + I_{135} + I_{90})/4 \\ s_1 &= I_0 - I_{90} \\ s_2 &= I_{45} - I_{135} \end{aligned} \quad (1a)$$

$$\begin{aligned} AoP &= \alpha = 0.5 \arctan(s_2/s_1) \\ DoPl &= \rho_l = \frac{\sqrt{s_2^2 + s_1^2}}{s_0} \end{aligned} \quad (1b)$$

From the raw images (640×460) captured by the camera, the sub-images can be extracted directly using super-pixel method that leads to four images, half of the size of the raw image, or can be interpolated to the full size [?, ?]. The super-pixel method was used for the results presented in this paper. Being interested in large-field of view, a fisheye lens of 180-degree was used on the camera, **information of the lens**.

An example of captured raw image, the linearly polarized images and subsequently the three stokes parameters and polarized information is shown in Fig. 2 & 3.

The IMPREX Bobcat GEV camera operates using eBus SDK-pleora driver and libraries [?]. To be able to use the camera integrated with other sensors, in the robotic field, we have created a ROS package, pleora-polarcam [?]. Initiating

from Iralab photonfocus driver [?], pleora-polarcam package is adapted for Imperex polarimetric cameras. Using this package the user can easily roslaunch or rosrun the camera and beside, buffering and saving the raw data, process the stokes and polarized parameters.

III. POLARIZED CUES USED FOR ATTITUDE ESTIMATION

A. Rayleigh scattering model

The unpolarized sunlight passing through our atmosphere gets scattered by different particles within the atmosphere. Beside deviating the direction of propagate wave, this transition also changes the polarization state of the incident light. This transition can be explained using Rayleigh scattering model. Rayleigh scattering describes the scattering of light or any electromagnetic waves by particles much smaller than their transmission wavelength. Accordingly it assumes that scattering particles of the atmosphere are small, homogeneous particles much smaller than the wavelength of the sunlight. Despite its simplification and assumption, this model proved to be sufficient for describing skylight scattering and polarization patterns [?, ?].

The Rayleigh model predicts that the unpolarized sunlight becomes linearly polarized after being scattered by the atmosphere. On the one hand, the Degree of linear Polarization is directly linked to the scattering angle (γ) according to:

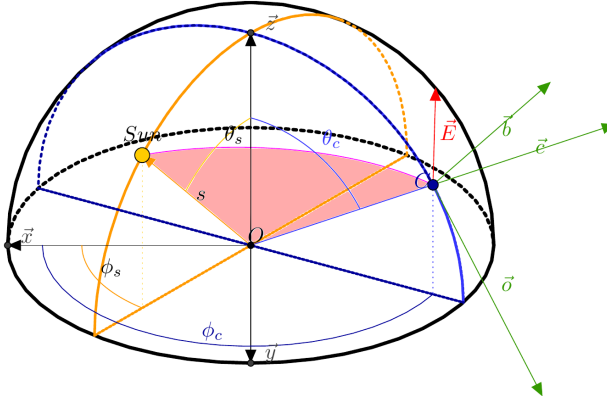


Fig. 4. Skylight polarization by scattering. Scattering plane is highlighted by light shade of red. (θ_s, ϕ_s) and (θ_c, ϕ_c) define the zenith and azimuth angle of sun and celestial point respectively. \widehat{obc} defines the pixel frame, \mathcal{P} , and \vec{E} is the electrical field orthogonal to the scattering plane.

$$\rho_l = \rho_{l_{max}} \frac{1 - \cos^2(\gamma)}{1 + \cos^2(\gamma)} \quad (2)$$

where $\rho_{l_{max}}$ is a constant that should be equal to 1 in theory but in practice the constant is slightly less than 1 due to some atmospheric disturbances[?]. The scattering angle γ is defined by the angle between the observed celestial vector \vec{c} and the sun vector \vec{s} as presented Fig. 4. It can be noticed that the Degree of Polarization is 0 in the sun direction and maximum when the scattering angle is $\pi/2$. [?, ?].

On the other hand, the scattered light is said polarized orthogonally to the scattering plane. Consequently, the Angle of Polarization is directly related to the orientation of the scattering plane.

B. Polarization by scattering model for sky pattern

As presented Fig. xx, an image is considered as a collection of pixels, and each pixel measures the polarization parameters of the light travelling along a ray associated with that pixel. The pixel frame \mathcal{P} is defined accordingly with the ray which coincides with \vec{c} . The camera calibration determines the relationship between pixels and these 3D rays.

Let's consider one pixel of the image with its associated pixel frame \mathcal{P} (\widehat{obc}). Based on Rayleigh scattering the electric field of incident light after scattering is perpendicular to the scattering plane, that is defined by the observer, celestial point and the sun. Accordingly the normalized electric field vector \vec{E} in the world frame is presented as the normalized cross product of \vec{s} and \vec{c} (see Eq. 3).

$$\vec{E} = \frac{\vec{s} \wedge \vec{c}}{\|\vec{s} \wedge \vec{c}\|} \quad (3)$$

The same measure in the pixel frame \mathcal{P} is represented as:

$$E_{obc} = \begin{bmatrix} E_o \\ E_b \\ 0 \end{bmatrix} = \begin{bmatrix} \cos \alpha \\ \sin \alpha \\ 0 \end{bmatrix} \quad (4)$$

where α is the measured AoP associated to the corresponding pixel. Combination of Eq. 3 & 4 and using the scattering angle γ , between \vec{s} and \vec{c} leads to:

$$\begin{cases} (\vec{s} \wedge \vec{c}) \cdot o = \sin \gamma \cos \alpha \\ (\vec{s} \wedge \vec{c}) \cdot b = \sin \gamma \sin \alpha \end{cases} \quad (5)$$

applying vector triplet cross product rule on Eq. 5 results.

$$\begin{cases} s \cdot b = \sin \gamma \cos \alpha \\ s \cdot o = -\sin \gamma \sin \alpha \end{cases} \quad (6)$$

Using Eq. 2, the scattering angle γ , therefore can be represented as:

$$\cos \gamma = s \cdot c = \pm \sqrt{\frac{1 - \rho'_l}{1 + \rho'_l}} \quad (7)$$

with $\rho'_l = \frac{\rho_l}{\rho_{l_{max}}}$.

Equations 6 & 7 finally leads to a representation of the sun vector in pixel frame \mathcal{P} which express a direct relation between the AoP, the scattering angle and the sun position:

$$\vec{s}_p = \begin{bmatrix} -\sin \gamma \sin \alpha \\ \sin \gamma \cos \alpha \\ \cos \gamma \end{bmatrix} \quad (8)$$

In another word, the sun vector is expressed in the pixel frame as a vector depending only on the polarization parameters AoP and DoPl (which is directly linked to the scattering angle γ).

C. UAV attitude and polarized sky pattern

This section presents how the information so far presented can be used for attitude estimation of an UAV. The overview of the considered scenario, the frame conventions and rotations for an UAV is shown in Fig. 5.

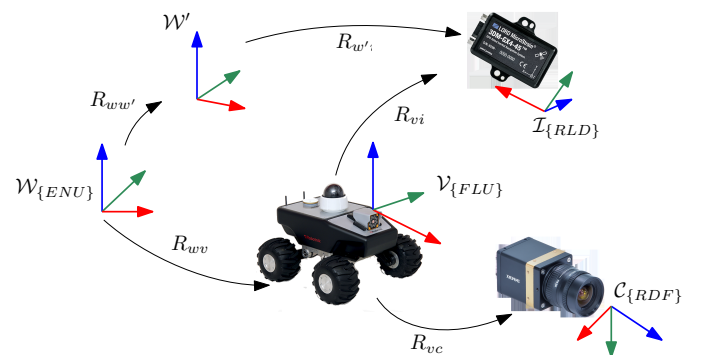


Fig. 5. Frame conventions and rotations for attitude estimation of an UAV -the figure needs to be changed pixel frame should be added, some parts can be removed.

In Fig. 5 the \mathcal{W} , \mathcal{W}' , \mathcal{I} , \mathcal{V} , \mathcal{C} , and \mathcal{P} , present the world frame, global frame of inertial measurement unit (IMU), IMU frame, vehicle frame, camera frame, and pixel frame respectively. Where the rotation from each frame to another is presented with lowercase alphabet. In the shown scenario,

a vector v_p in pixel frame is expressed in the world frame, v_w :

$$v_w = R_{wv} \cdot R_{vc} \cdot R_{cp} \cdot v_p \quad (9)$$

where the rotation from the camera to the pixel frame R_{cp} is defined as the yaw and pitch rotation by the zenith and azimuth angle of the celestial point (θ_c, ϕ_c) as shown in Eq. 10.

$$\begin{aligned} R_{cp} &= \begin{bmatrix} \cos \theta_c \cos \phi_c & -\sin \phi_c & \sin \theta_c \cos \phi_c \\ \cos \theta_c \sin \phi_c & \cos \phi_c & \sin \theta_c \sin \phi_c \\ -\sin \theta_c & 0 & \cos \theta_c \end{bmatrix} \quad (10) \\ &= R_{z_c}(\phi_c) \cdot R_{y_c}(\theta_c) \end{aligned}$$

Previously we presented how to express sun position in pixel frame (see Eq. 8). Indeed this representation is applied to any point from world frame, ergo:

$$\begin{aligned} s_w &= R_{wv} \cdot R_{vc} \cdot R_{cp} \cdot \begin{bmatrix} -\sin \gamma \sin \alpha \\ \sin \gamma \cos \alpha \\ \cos \gamma \end{bmatrix} = R_{wv} \cdot R_{vc} \cdot v \\ R^T \cdot s_w &= v \end{aligned} \quad (11)$$

In the above equation, α , R_{cp} , and R_{vc} are known, however to find the R_{wv} , γ should be estimated. How to estimate this parameter and definition of absolute and relative attitude estimation is explained in next Sect. IV.

IV. ATTITUDE ESTIMATION

This section explains how to estimate scattering angle (γ), absolute and relative rotation of the UAV in world frame (R_{wv}).

A. γ estimation

Considering that we are only measuring the angle of polarization α in scattering effects, we have to estimate γ to get the vector v defined in Eq. 11. This equation is valid for all the points in sky region. However with only two celestial points, γ can be estimated as expressed in the following.

$$\begin{cases} R^t \cdot s = R_{cp_1} \cdot \begin{bmatrix} -\sin \gamma_1 \sin \alpha_1 \\ \sin \gamma_1 \cos \alpha_1 \\ \cos \gamma_1 \end{bmatrix} \\ R^t \cdot s = R_{cp_2} \cdot \begin{bmatrix} -\sin \gamma_2 \sin \alpha_2 \\ \sin \gamma_2 \cos \alpha_2 \\ \cos \gamma_2 \end{bmatrix} \end{cases} \quad (12)$$

Using the product of R_{cp} and $R_z(\alpha)$, Eq. 12 is rewritten as:

$$M_1 \cdot \begin{bmatrix} 0 \\ \sin \gamma_1 \\ \cos \gamma_1 \end{bmatrix} = M_2 \cdot \begin{bmatrix} 0 \\ \sin \gamma_2 \\ \cos \gamma_2 \end{bmatrix} \quad (13)$$

By defining the matrix M such that $M = M_2^t \cdot M_1$, γ_1 and γ_2 are found as:

$$\begin{cases} \gamma_1 = -\arctan \frac{M_{02}}{M_{01}} \\ \gamma_2 = -\arctan \frac{M_{20}}{M_{10}} \end{cases} \quad (14)$$

The AoP is 2π modulus, while the γ found in Eq. 14 is π modulus, this leads to two possible solutions for vector v , (α_1, γ_1) and $(\alpha_1 + \pi, -\gamma_1)$.

B. Absolute rotation

In order to estimate the absolute rotation and attitude of the UAV, it is assumed that: (i) the sun position is known, (ii) using the AoP measures of the sky (2 points), the vector v is estimated, (iii) either using the AoP from horizontally reflected areas (i.e. water) a second vectors w is estimated or the vertical in the pixel frame is known. In this study we assumed that the vertical in the pixel frame is known, however having any horizontal surface, the second vector can be estimated.

The aforementioned assumptions leads to the following expression, where z is the vertical in world frame $([0, 0, 1])$ and t is the time instance.

$$\begin{cases} [s, z, s \wedge z] = R(t) \cdot [v(t), w(t), v(t) \wedge w(t)] \\ = R_{wv}(t) \cdot R_{vc} \cdot [v(t), w(t), v(t) \wedge w(t)] \end{cases} \quad (15)$$

Solving Eq. 15 enables to get $R_{wv}(t)$. However due to γ ambiguities, there exist two solutions for v and therefore for R_{wv} . To constraint the solutions, at each time stamp, a closest solution compare to the previous time stamp is selected.

C. Relative rotation

The relative rotation is estimated between two different time stamps (t_1, t_2) , Therefore Eq. 15 becomes (For simplicity in the rest, $v(t_1)$ and $v(t_2)$ are referred as v_1 and v_2):

$$\begin{cases} [s, z, s \wedge z] = R_{wv_1} \cdot R_{vc} \cdot [v_1, w_1, v_1 \wedge w_1] \\ [s, z, s \wedge z] = R_{wv_2} \cdot R_{vc} \cdot [v_2, w_2, v_2 \wedge w_2] \end{cases} \quad (16)$$

which leads to:

$$R_{wv_2} = R_{wv_1} \cdot R_{vc} \cdot [v_1, w_1, v_1 \wedge w_1] \cdot [v_2, w_2, v_2 \wedge w_2]^{-1} \cdot R_{vc}^T \quad (17)$$

Using the above equation, the relative rotation $R_{v_1 v_2}$ is equal to:

$$R_{v_1 v_2} = R_{vc} \cdot [v_1, w_1, v_1 \wedge w_1] \cdot [v_2, w_2, v_2 \wedge w_2]^{-1} \cdot R_{vc}^T \quad (18)$$

In this section we explained the basic theory of attitude estimation based on polarization by scattering. This theory, however needs to be tested which is explained in the next section.

V. EXPERIMENTS AND RESULTS

This section presents our setup, the designed experiments, the obtained results, the difficulties faced during the experiments and our provided solutions.

The setup used in our experiment is based on fig. 5. However instead of UAV, a camera tripod was used (see Fig. 6).



Fig. 6. The setup used for acquiring presented datasets in this paper

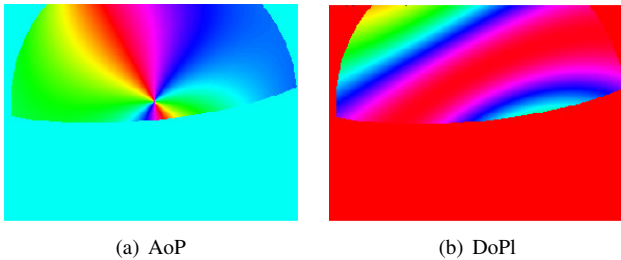


Fig. 7. Synthetically created AoP and DoPI images of sky region for yaw, pitch and roll angle of 1.8, -0.2 and 0.1, respectively.

For the presented experiments, we considered that R_{vi} between IMU and UAV, as well as initial pose of the UAV in the world frame were identity. To be able to using the IMU recordings as ground-truth (GT), this device was calibrated with the camera using kalibr toolbox [?, ?]. The polarimetric camera with fisheye lens was also calibrated according to [?]. Using the explained setup a dataset of synthetic images was created. Indicating that AoP and DoPI images for sky regions were synthetically created using the IMU recordings obtained during real acquisition. Figure 7 shows an example of this dataset at optimal conditions.

Applying our framework on ideal synthetic data, perfect results were obtained for absolute and relative rotations, while γ was estimated using only two random points from sky region (see Fig. 8). As illustrated in Fig. ??, the synthetic dataset, created based on IMU recordings, has rotation of roll, pitch and yaw, respectively. This dataset has 856 samples, however for simplicity, it has being down sampled by sampling rate of 30 samples.

Although using our proposed framework we were able to achieve perfect results on ideal synthetic data, in reality it is rare to obtain the perfect skylight polarization pattern. Variety of causes clutter the desired skylight pattern, main one being pollution. To account for such cases, a second experiment was performed while significant level of noise was added to the created synthetic data. Figure 9 shows the an example of synthetic data with %10 noise.

Performing the same 2-random-point algorithm as before on noisy dataset leads to the results illustrated in Fig. 10(a). As expected the performance decline, simply due to the noise.

To solve this problem, we defined two ransac models for the absolute and relative rotation, respectively. In the proposed ransac model for absolute rotation, since the sun

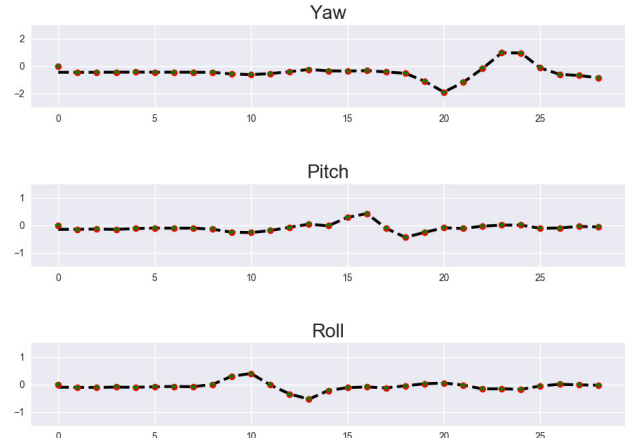


Fig. 8. Absolute and relative rotation obtained from synthetic data in optimal conditions. The black line represents the GT, the dots and the stars represent the absolute and relative predicted rotations, respectively.

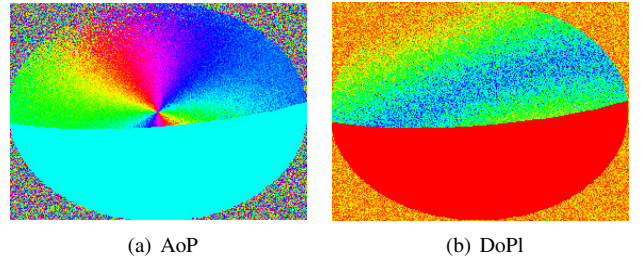


Fig. 9. Synthetically created AoP and DoPI images of sky region with noise level of 0.1. With yaw, pitch and roll angle of 1.8, -0.2 and 0.1, respectively.

position is known the ransac model optimizes the full rotation of each frame in comparison to the origin considering the difference between the predicted and real sun positions.

The relative model, however, there is no information about the original position, or sun position, and the algorithm only depends on the polarized vector, $v = R_{cp} * v_p$ between two different frames. Therefore using the ransac model, the optimal vector representing each frame is obtained.

Running our ransac models on the noisy datasets, with error threshold of 0.07, 10 random points (2 points for defining the model and the rest as test), and 2000 iterations the following results are obtained:

The quantitative results in terms of mean difference (μ) and standard deviation (σ) between the predicted rotations and GT are tabulated in Table. I.

TABLE I
MEAN DIFFERENCE AND STANDARD DEVIATION COMPARISON BETWEEN PREDICTED RESULTS AND GT IN RADIAN.

	Yaw		Pitch		Roll	
	μ	$\pm\sigma$	μ	$\pm\sigma$	μ	$\pm\sigma$
Absolute	0.087	0.078	0.020	0.029	0.068	0.100
Relative	0.275	0.35	0.113	0.123	0.148	0.111

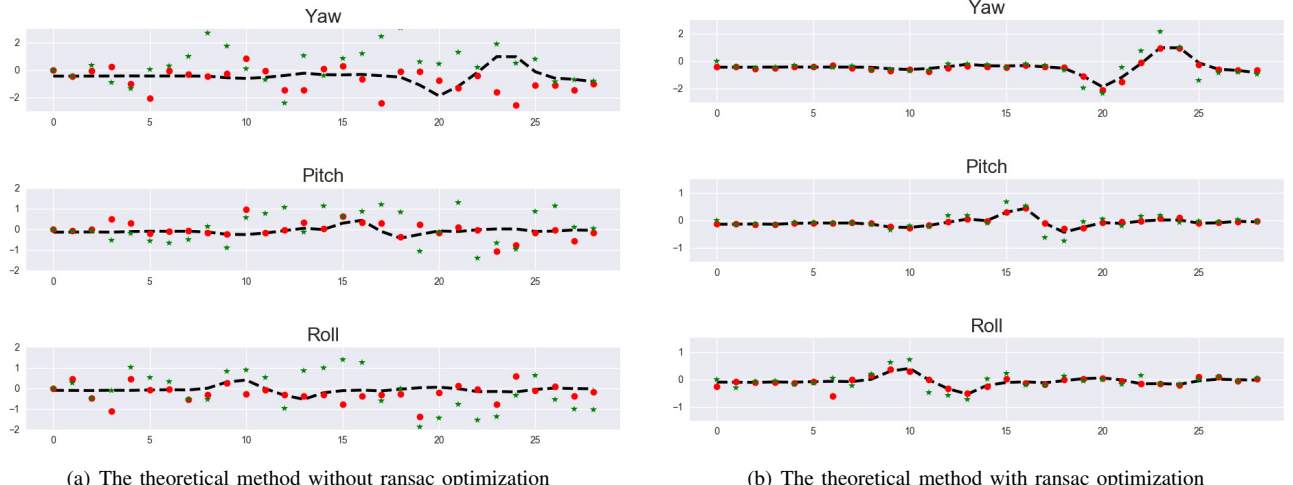


Fig. 10. Absolute and relative rotation obtained from noisy synthetic data without and with ransac optimization. The black line represents the GT, the dots and the stars represent the absolute and relative predicted rotations, respectively.

The mean difference and standard deviation between predicted rotations and GT

As illustrated in Fig. 10(b), using the ransac model the outliers are ignored and satisfactory results are achieved.

VI. DISCUSSION AND CONCLUSION

This paper presents the primary results of our attitude estimation using polarimetric camera on the generated synthetic data. Two sets of data were generated one considering optimal and another noisy (more realistic) conditions. In order to cope with the undesired artifacts and outliers in the measurements, we integrated a ransac model in our framework which resulted in a satisfactory performance.

To be continued.